Semiconductor Physics, Quantum Electronics & Optoelectronics, 2026. V. 29, No 2. P. 219-227.

Optoelectronics and optoelectronic devices

Propagation dynamics of radially polarized terahertz vortex beams

A.V. Degtyarev, M.M. Dubinin*, O.V. Gurin, V.O. Maslov, K.I. Muntean, V.N. Ryabykh

V.N. Karazin Kharkiv National University, 4 Svobody Square, 61022 Kharkiv, Ukraine
**Corresponding author e-mail: mykola.dubinin@karazin.ua*

Abstract. Analytical expressions to describe nonparaxial diffraction of vortex laser beams during their propagation in free space are obtained. The beams excited by radially polarized TM_{0m} (m = 1, 2, 3) modes of a dielectric waveguide resonator of a terahertz laser, which interact with a spiral phase plate with an arbitrary topological charge (n) are considered. The simulation is performed using the Rayleigh–Sommerfeld integral theory. It is shown that a phase plate with topological charges n = 1, 2 forms a field in the Fresnel zone, in which an azimuthal component appears. In this case, preservation of the radial and longitudinal components of the field is observed and the contribution of the longitudinal component to the total beam power remains insignificant. For a phase plate charge n = 1, the maximum of the field intensity is located on the axis, whereas the field distribution for n = 0 and n = 2 becomes ring-shaped. The maximum values of the field intensity are observed at a charge n = 1, while they decrease at n = 2. Phase distributions of the field transverse components of vortex laser beams are visualized. At a topological charge n = 1, they become a one-lobe helical structure, and a two-lobe structure with more pronounced helical twists of the azimuthal component for all the studied modes is observed at n = 2.

Keywords: vortex beam, terahertz laser, dielectric resonator, modes, phase plate, propagation.

https://doi.org/10.15407/spqeo29.02.219
PACS 42.55.-f, 42.60.Da, 42.60.-v, 42.62.-b

Manuscript received 04.11.25; revised version received 04.05.26; accepted for publication 10.06.26; published online 23.06.26.

1. Introduction

The terahertz (THz) frequency range is an intermediate region of the electromagnetic spectrum between the infrared and microwave ranges. One of the essential properties of THz radiation is its non-ionizing character, setting it apart from X-ray radiation [1]. The spectra of complex organic compounds, including protein molecules, DNA, and various explosives, fall within the terahertz range [2]. In this spectral range, dry dielectric materials such as fabrics, wood, paper and plastics exhibit high transparency. Terahertz laser radiation provides a promising basis for developing more efficient scanning systems used in security inspection procedures. Use of this type of radiation enables detection of nonmetallic objects concealed under clothing, including ceramic weapons, drugs, and explosives, without causing harmful effects to the human body [3]. Use of THz lasers has become widespread in industry, especially for non-destructive testing and quality assessment of materials [4]. THz technologies enable efficient detection of defects, cracks, and damage in composite materials, plastic products, and ceramics, as well as harmful substances in food products [5–7]. In the terahertz range, resonances associated with rotational and vibrational transitions of many molecules are observed, providing valuable spectroscopic information. Analysis of these resonances enables identification of molecules based on their unique spectral characteristics, which act as molecular "fingerprints" [8, 9]. The terahertz range is also considered one of the most promising frequency domains for future 6G wireless communication technologies, which are expected to involve device operation within this spectral region [10–13].

Among terahertz laser beams, vortex beams are of particular interest due to their unique properties, which confer significant importance in various applications. The most prominent feature of the vortex beams is the spiral configuration of the wavefront, enabling realization of orbital angular momentum with numerous states and supplementary degrees of freedom. In this case, the surface of constant phase is not a plane but a complex helix-shaped three-dimensional structure – a helicoid [14]. At the same time, a singularity corresponding to an undefined phase form along the beam axis (at the center). As a result, the intensity of such beams drops to zero at the beam axis. However, the energy is not entirely lost. Instead, it is redistributed around the axis, forming a ring-shaped intensity profile [15].

There are two key methods for generating terahertz vortex beams. One approach uses specialized external

devices to modulate the wavefront, while the other achieves direct excitation of vortex beams inside the laser cavity. In the first method, wavefront modulation is achieved using various optical components such as achromatic polarizing elements, spiral phase plates, and computer-generated holograms [16–19]. Vortex beams can be generated directly in a laser resonator by employing either optical rectification or difference-frequency generation techniques [20–23].

Optically pumped terahertz molecular lasers are among the first and most efficient sources of terahertz radiation [24, 25]. They utilize a line-tunable CO_2 laser to selectively excite specific transitions in a molecular gas, thereby producing rotational population inversion within a tunable optical cavity. Waveguide resonators are commonly used in optically pumped lasers, as they allow generation of high continuous-wave powers within relatively small cavities. Among the modes of such resonators, the TM_{0m} modes with radial field polarization have a region of strong longitudinal electric field in the focus. The longitudinal field modes carrying orbital angular momentum are of considerable interest for increasing the information capacity and spectral efficiency of wireless communication lines in the terahertz frequency range [26]. Wave beams of this type can be efficiently generated using spiral phase plates [27].

In this paper, we develop analytical expressions for describing nonparaxial diffraction of radially polarized TM_{0m} modes formed in a dielectric waveguide resonator of a terahertz laser upon interaction with a spiral phase plate. The spatial structure and evolution of the intensity and phase of the induced optical vortices are analyzed.

2. Theoretical model

Vectorial Rayleigh–Sommerfeld integrals [28–30] or the plane-wave expansion technique [31–33] are employed to study propagation of radiation in free space. For this case, nonparaxial approximation of the Rayleigh–Sommerfeld integrals is applied. The nonparaxial approximation yields greater precision than the traditional paraxial approximation. The first-kind vector form of the Rayleigh–Sommerfeld integral theorem in cylindrical coordinates is expressed as follows:

$$E_r(\rho_1,\beta,z_1)=-\frac{iz_1}{\lambda r_1^2}\exp(ikr_1)\int_0^{\infty}\int_0^{2\pi}[E_r^0(\rho_0,\varphi)\times$$
$$\times\cos(\varphi-\beta)-E_\varphi^0(\rho_0,\varphi)\sin(\varphi-\beta)]\times$$
$$\exp\left(ik\frac{\rho_0^2}{2r_1}\right)\exp\left(-ik\frac{\rho_1\rho_0\cos(\varphi-\beta)}{r_1}\right)\rho_0\,d\rho_0\,d\varphi, \quad (1.1)$$

$$E_\varphi(\rho_1,\beta,z_1)=-\frac{iz_1}{\lambda r_1^2}\exp(ikr_1)\int_0^{\infty}\int_0^{2\pi}[E_r^0(\rho_0,\varphi)\times$$
$$\times\sin(\varphi-\beta)+E_\varphi^0(\rho_0,\varphi)\cos(\varphi-\beta)]\times$$
$$\exp\left(ik\frac{\rho_0^2}{2r_1}\right)\exp\left(-ik\frac{\rho_1\rho_0\cos(\varphi-\beta)}{r_1}\right)\rho_0\,d\rho_0\,d\varphi, \quad (1.2)$$

$$E_z(\rho_1,\beta,z_1)=\frac{-i}{\lambda r_1^2}\exp(ikr_1)\int_0^{\infty}\int_0^{2\pi}\left\{\begin{bmatrix}E_r^0(\rho_0,\varphi)\begin{bmatrix}\rho_0-\\ \rho_1\cos(\varphi-\beta)\end{bmatrix}\\ +E_\varphi^0(\rho_0,\varphi)\rho_1\sin(\varphi-\beta)\end{bmatrix}\right\}\times$$
$$\times\exp\left(ik\frac{\rho_0^2}{2r_1}\right)\times\exp\left(-ik\frac{\rho_1\rho_0\cos(\varphi-\beta)}{r_1}\right)\rho_0\,d\rho_0\,d\varphi, \quad (1.3)$$

where $k=2\pi/\lambda$ is the wave number, λ is the wavelength, (ρ_0, φ) are the polar coordinates in the area where the input field is specified, (ρ_1,β,z_1) are the cylindrical coordinates in the observation plane, $E_r^0(\rho_0,\varphi)$ and $E_\varphi^0(\rho_0,\varphi)$ are the complex amplitudes of the r and φ components of the input electric field, respectively, and $r_1=\sqrt{\rho_1^2+z_1^2}$.

It is assumed in the framework of the theoretical model that the mode structure of the studied dielectric resonator coincides with the mode structure of a hollow circular dielectric waveguide. Let us define a radially polarized field in the form of TM_{0m} modes in the initial plane. In the source plane ($z_1 = 0$), the cylindrical components of the electromagnetic fields of these modes can be expressed as follows [34]:

$$\begin{cases}E_r^0(\rho_0,\varphi)=B_{01}J_1\left(U_{0m}\dfrac{\rho_0}{a}\right),\\ E_\varphi^0(\rho_0,\varphi)=0,\end{cases} \quad (2)$$

where a is the waveguide radius, J_1 is the Bessel function of the 1st kind of the first order, U_{0m} are the roots of the equation $J_1(x)=0$, and $B_{0m}=\dfrac{1}{a\sqrt{\pi}J_0(U_{0m})}$ are the normalizing factors for TM_{0m} modes, respectively.

We consider interaction of these modes with a spiral phase plate (SPP) characterized by an arbitrary topological charge n [35]. The spiral phase plate is placed at the output of the waveguide and has the same diameter as the waveguide aperture (Fig. 1). The complex transmission function for the given SPP characterized by a radius a and expressed in polar coordinates is presented in the following form [36]:

$$T_n(\rho_0,\varphi)=\mathrm{circ}\left(\frac{\rho_0}{a}\right)\exp(in\varphi)=\begin{cases}\exp(in\varphi), & \rho_0\le a,\\ 0, & \rho_0>a,\end{cases} \quad (3)$$

where $\mathrm{circ}\left(\dfrac{\rho_0}{a}\right)$ is the circular function.

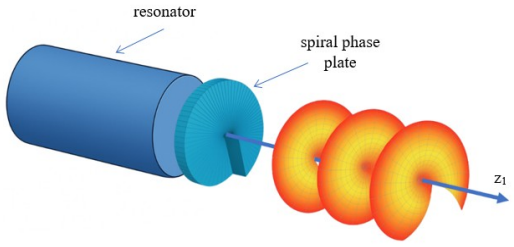

Fig. 1. Modeling scheme of laser beam propagation.

Integration of (2) over the angle φ can be efficiently performed using the following relations for integer μ > 0 [37]:

$$\int_0^{2\pi} \cos(\mu\varphi+\varphi_0)\exp\left[-ix\cos(\varphi-\theta)d\varphi\right]= \\ =2\pi(-i)^{\mu}J_{\mu}(x)\cos(\mu\varphi+\varphi_0),$$

$$\int_0^{2\pi} \sin(\mu\varphi+\varphi_0)\exp\left[-ix\cos(\varphi-\theta)d\varphi\right]= \\ =2\pi(-i)^{\mu}J_{\mu}(x)\sin(\mu\varphi+\varphi_0).$$

From the previous expressions, we arrive at the following relation:

$$\int_0^{2\pi} e^{-ix\cos(\varphi-\beta)}e^{in\varphi}d\varphi=2\pi e^{in\beta}(-i)^n J_n(x). \quad (4)$$

Applying Euler's formulas and taking Eq. (4) into account, we obtain the following expressions:

$$\int_0^{2\pi} e^{-ix\cos(\varphi-\beta)}e^{in\varphi}\sin\varphi d\varphi= \\ =-\pi e^{in\beta}(-i)^n\left[e^{i\beta}J_{n+1}(x)+e^{-i\beta}J_{n-1}(x)\right], \quad (5.1)$$

$$\int_0^{2\pi} e^{-ix\cos(\varphi-\beta)}e^{in\varphi}\cos\varphi d\varphi= \\ =\pi e^{in\beta}(-i)^{n+1}\left[e^{i\beta}J_{n+1}(x)-e^{-i\beta}J_{n-1}(x)\right]. \quad (5.2)$$

By applying (5.1) and (5.2), we derive the following expressions for the field components describing nonparaxial diffraction of the TM_{0m} modes on SPP:

$$E_r(\rho_1,\beta,z_1)=\frac{(-i)^{n+2}kz_1}{2r_1^2}e^{i(n\beta+kr_1)}B_{0m}\times \\ \times\left[I1_{1n+1}(\rho_1,z_1)-I1_{1n-1}(\rho_1,z_1)\right], \quad (6.1)$$

$$E_{\varphi}(\rho_1,\beta,z_1)=\frac{(-i)^{n+3}kz_1}{2r_1^2}e^{i(n\beta+kr_1)}B_{0m}\times \\ \times\left[I1_{1n+1}(\rho_1,z_1)+I1_{1n-1}(\rho_1,z_1)\right], \quad (6.2)$$

$$E_z(\rho_1,\beta,z_1)=\frac{(-i)^{n+1}k}{2r_1^2}e^{i(n\beta+kr_1)}B_{0m}\times \\ \times\left\{2I2_{1n}(\rho_1,z_1)+i\rho_1\left[I1_{1n+1}(\rho_1,z_1)-I1_{1n-1}(\rho_1,z_1)\right]\right\}, \quad (6.3)$$

where the following notations are defined:

$$I1_{1n}(\rho_1,z_1)=\int_0^a J_1\left(U_{0m}\frac{\rho_0}{a}\right)J_n\left(\frac{k\rho_1\rho_0}{r_1}\right)\times \\ \times\exp\left(ik\frac{\rho_0^2}{2r_1}\right)\rho_0\,d\rho_0,$$

$$I2_{1n}(\rho_1,z_1)=\int_0^a J_1\left(U_{0m}\frac{\rho_0}{a}\right)J_n\left(\frac{k\rho_1\rho_0}{r_1}\right)\times \\ \times\exp\left(ik\frac{\rho_0^2}{2r_1}\right)\rho_0^2\,d\rho_0.$$

3. Results and discussion

Theoretical calculations of the intensity distributions $I=|E_r|^2+|E_\varphi|^2+|E_z|^2$ and phase characteristics $\varphi_i=\mathrm{arctg}(\mathrm{Im}(E_i)/\mathrm{Re}(E_i)), i=r,\varphi,z)$ of the vortex laser beam field were performed using the expressions (6). The beams excited by radially polarized TM_{0m} (m = 1, 2, 3) modes of a dielectric waveguide resonator of a terahertz laser during beam propagation in free space were considered. A spiral phase plate was installed at the output of the waveguide resonator to form the studied vortex beams. The waveguide and SPP had identical diameters of 35 mm. In the calculations, the radiation wavelength was λ = 0.4326 mm, which corresponds to the generation line of an HCOOH laser with optical pumping [38]. In this work, the spatial-energy properties of the field of the studied beams were compared for the values of the topological charge of SPP n = 0, 1, 2.

Fig. 2 shows the longitudinal and transverse distributions of the total intensity of the field of laser beams excited by TM_{01}, TM_{02}, TM_{03} modes in free space. Calculations of the longitudinal distributions of the field intensity were carried out in the Fresnel diffraction zone for the distances z_1 = 100…700 mm, and the transverse distributions were considered in the areas of the maximum field intensity. It can be seen from Fig. 2 that field distribution of the beams excited by the considered modes in free space is governed by both the mode order and the topological charge. For topological charges n = 0 (in the absence of SPP) and n = 2, the transverse profiles have pronounced ring structures, whereas for the charge n = 1, the intensity is concentrated on the axis.

In order to obtain quantitative description of the transverse structure of the beams at the planes where the intensity reaches its maximum, the effective diameter was computed using the following expression:

$$d_s=2\sqrt{\frac{2\int_0^{2\pi}\int_0^{\infty}\rho_1^2 I(\rho_1,\beta,z_1)\rho_1 d\rho_1 d\beta}{\int_0^{2\pi}\int_0^{\infty}I(\rho_1,\beta,z_1)\rho_1 d\rho_1 d\beta}}.$$

The results of the calculations of the diameter and the coordinate z_1 for the plane of the maximum intensity I_{max} are presented in Table. For each of the modes, the highest values of the maximum intensity correspond to a single topological charge, whereas for a charge n = 2, the intensity is significantly lower. The intensity maximum planes for all the beams under study at n = 1 are located farther from the source: for the TM_{01} mode at a distance of about 527 mm, for the TM_{02} mode – 321 mm, and for the TM_{03} mode – 230.5 mm. This distance decreases significantly at increasing the mode order. The smallest beam diameter in the plane of the maximum intensity is observed in the absence of the topological charge (29.54 and 34.38 mm, respectively) for the TM_{01} and TM_{03} modes and at the charge n = 2 (30.46 mm) for the TM_{02} mode. The highest values for all the considered modes are characteristic for the topological charge n = 1, where the diameter reaches more than 38 mm.

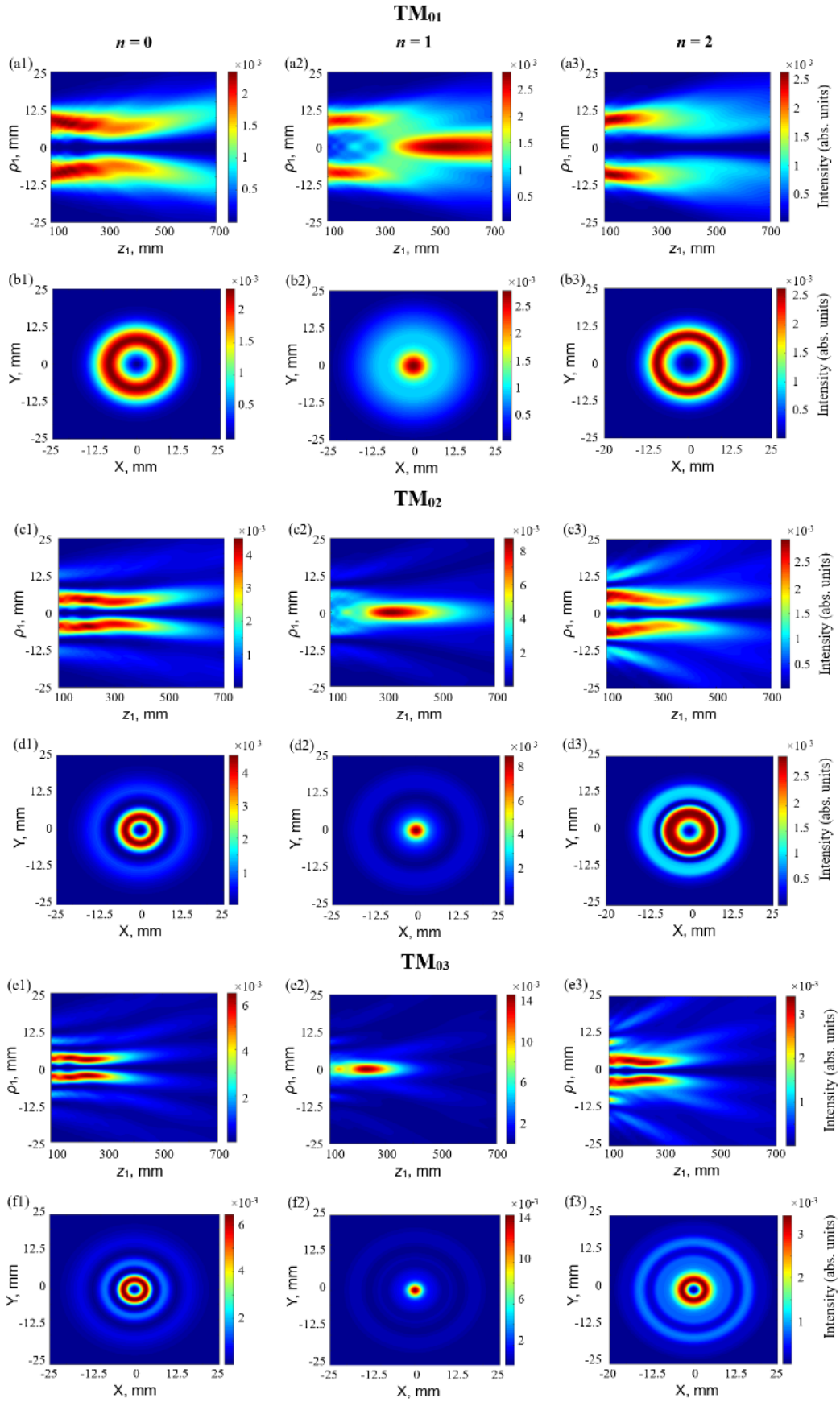

Fig. 2. Longitudinal (a1–a3, c1–c2, e1–e3) and transverse (b1–b3, d1–d3, f1–f3) intensity distributions of vortex laser beams excited by TM_{0m} (m = 1, 2, 3) modes in free space.

Table. Spatial-energy characteristics of laser beams excited by TM_{0m} modes at different topological charges.

Mode	n	z_1, mm	$I_{max}\cdot10^{-3}$, abs. un.	Beam diameter d, mm
TM_{01}	0	175.5	2.35	29.54
	1	527	2.84	38.74
	2	131	2.65	29.87
TM_{02}	0	207.5	4.49	32.89
	1	321	8.68	39.75
	2	100	2.99	30.46
TM_{03}	0	167.5	6.46	34.38
	1	230.5	14.64	40.11
	2	171.5	3.43	37.82

To study spatial distribution of the field components, the dependences of their relative contributions $\eta(z_1)$ to the laser beam power in the Fresnel diffraction zone for topological charges n = 1, 2 were calculated using the following expression:

$$\eta(z_1)=\frac{\int_0^{2\pi}\int_0^{\infty}\left|E_{r,\varphi,z}(\rho_1,\beta,z_1)\right|^2\rho_1 d\rho_1 d\beta}{\int_0^{2\pi}\int_0^{\infty}\left[\begin{matrix}\left|E_r(\rho_1,\beta,z_1)\right|^2+\left|E_\varphi(\rho_1,\beta,z_1)\right|^2\\+\left|E_z(\rho_1,\beta,z_1)\right|^2\end{matrix}\right]\rho_1 d\rho_1 d\beta}.$$

In the absence of a spiral phase plate, the total field intensity is formed by the radial E_r and longitudinal E_z field components (Fig. 3). At the same time, the contribution of the E_z component for all the studied topological charges to the total beam power turned out to be small. Therefore, the $\eta(z_1)$ graph as well as the intensity and phase distributions for this component are not presented further.

The graphs show that the contribution of the radial component to the laser beam power for the TM_{01} mode decreases at increasing the distance from the source while the contribution of the azimuthal component increases. For a topological charge n = 2, this tendency leads to the fact that starting from distances of about 550 mm, the contribution of the E_φ component becomes dominant. For the TM_{02} mode at n = 1, the contribution of the E_r component decreases at increasing the distance from the source to ~ 400 mm, while the relative contribution of the E_φ component increases. Then the contribution of the E_r component increases again, while the contribution of the E_φ component gradually decreases. At a charge n = 2, a pronounced intermediate region is observed, in which the contributions of the radial and azimuthal components of the field at the distances of about 400…600 mm are practically equal. For the TM_{03} mode at n = 1, 2, the radial component remains dominant over the entire range of distances, showing only minor fluctuations. The contribution of the E_φ component has a moderate maximum at a distance of about 300 mm, after which it gradually decreases.

Fig. 4 shows transverse distributions of intensity (a1, a2, c1, c2) and phase (b1, b2, d1, d2) of individual field components for beams excited by the TM_{01} mode

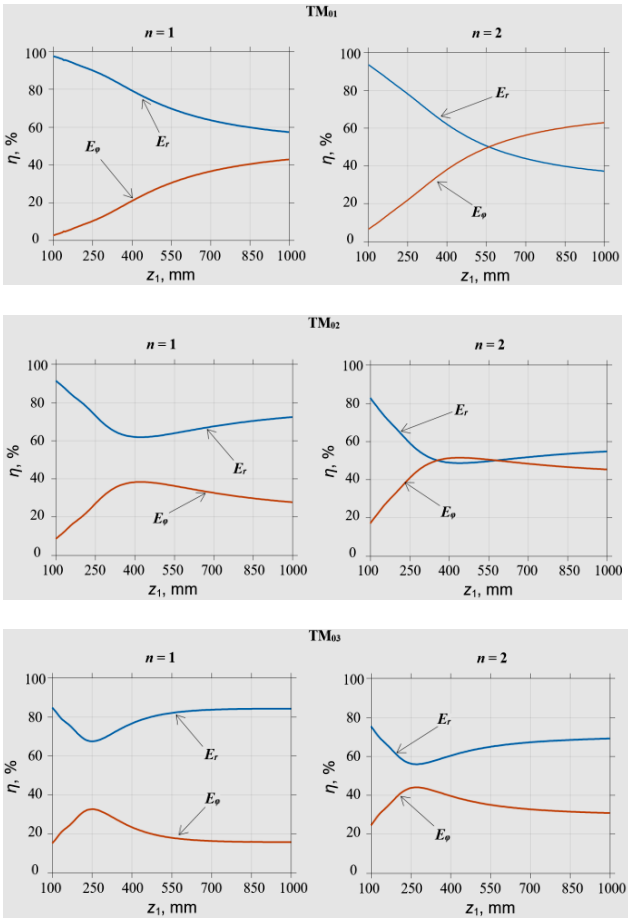

Fig. 3. Dependences of the relative contributions η of the field components of vortex laser beams, excited by TM_{01}, TM_{02}, and TM_{03} modes, to the total power.

in the planes of maximum intensity values. For a topological charge n = 1, both transverse components have a maximum on the axis with the E_r profile having a large transverse extent and the E_φ profile concentrated in the central region. The phase distributions exhibit a helical one-lobed structure. Change in the topological charge from 1 to 2 is accompanied by both transformation of the transverse profile from the axis-centered region of maximum intensity to a ring structure for both components and a increase in the vortex petal structure of the phase in accordance with the topological charge.

For laser beams excited by the TM_{02} mode at a topological charge of n = 1, the intensity of the radial component has a maximum on the axis and a weakly defined ring, while the intensity of the azimuthal component is concentrated in the axial region (Fig. 5). At a charge n = 2, the transverse profile of the E_r component is transformed into a pronounced two-ring structure, and the similar profile of the E_φ component is transformed into a single-ring structure. The phase distributions show a vortex structure for both components: one-lobed at n = 1 and two-lobed at n = 2. Moreover, phase distributions of the azimuthal component are characterized by a large number of spiral twists.

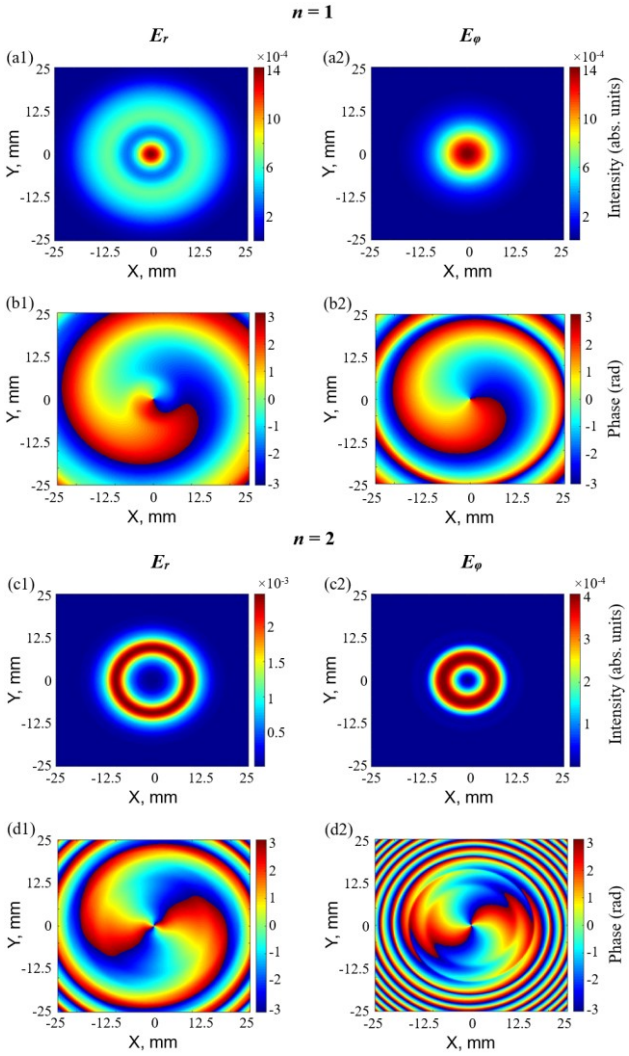

Fig. 4. Transverse intensity (a1, a2, c1, c2) and phase (b1, b2, d1, d2) distributions of the field components for laser beams excited by the TM_{01} mode.

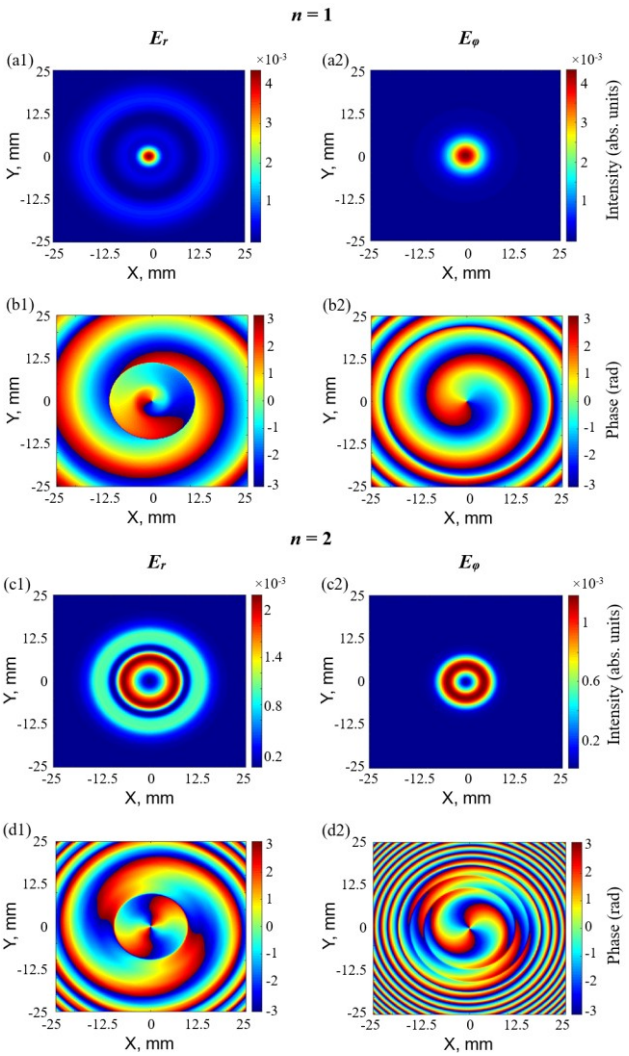

Fig. 5. Transverse intensity (a1, a2, c1, c2) and phase (b1, b2, d1, d2) distributions of the field components for laser beams excited by the TM_{02} mode.

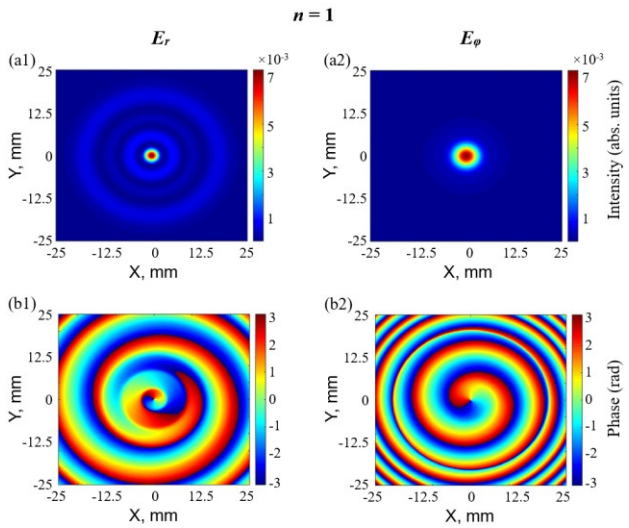

Fig. 6. Transverse intensity (a1, a2, c1, c2) and phase (b1, b2, d1, d2) distributions of the field components for laser beams excited by the TM_{03} mode.

Fig. 6 shows the transverse intensity distributions (top row) and phase (bottom row) of individual field components for beams excited by the TM_{03} mode. At a charge $n = 1$, the intensity of the radial component has an axial maximum with a series of weak concentric rings, while the profile of the azimuthal component is more compact and localized near the axis. At a charge $n = 2$, the E_r profile transforms into a multi-ring structure, and E_φ acquires a clear single-ring shape. The phase distributions exhibit a vortex lobe structure: one-lobe for $n = 1$ and two-lobe for $n = 2$.

4. Conclusions

In this work, analytical expressions for describing non-paraxial diffraction of vortex beams excited by radially polarized modes TM_{0m} ($m = 1, 2, 3$) of a dielectric waveguide resonator during beam propagation in free space are obtained. The calculations used the Rayleigh–Sommerfeld theory. Formation of the vortex beams was carried out by a spiral phase plate of arbitrary topological charge n.

It is shown that for charges $n = 0$ and $n = 2$, the transverse profiles of the radiation beam have a pronounced ring structure, whereas for the charge $n = 1$, the maximum of the field is observed on the axis. In the absence of SPP, the field distribution in free space for the TM_{0m} modes is formed by the radial and longitudinal components. In case of using SPP, an azimuthal component appears in the field distribution. However, contribution of this component to the total power turned out to be insignificant in all the cases.

For each of the modes, the highest values of the field intensity in free space correspond to a single topological charge, whereas for a charge $n = 2$, these values are significantly lower. The intensity maxima for the charge $n = 1$ are located farther from the source and shift towards it at increasing the mode order.

It is found out that distributions of the transverse components of the field at the SPP charge $n = 1$ have a maximum on the axis. For the azimuthal component, the field localizes near the axis, while the field expansion is observed for the radial component. Phase distributions of the field have a one-lobed helical structure. At $n = 2$, the field intensity profiles are transformed from axial to annular. Moreover, with an increase in the mode order, the field distribution of the azimuthal component remains localized in a ring, while for the radial component the number of such rings increases. At the same time, the phase profile changes from one to two lobes, proportional to the topological charge, and the azimuthal component distributions contain more spiral twists.

References

1. Rieh J.-S. *Introduction to Terahertz Electronics*. Springer Cham., 2021. https://doi.org/10.1007/978-3-030-51842-4.
2. Wang R., Hao R., Li D. *et al.* Multifunctional terahertz biodetection enabled by resonant metasurfaces. *Adv. Mater*. 2025. **37**, No 16. P. 2418147. https://doi.org/10.1002/adma.202418147.
3. Wang B., Wang H., Bao Y. *et al.* Sustainable materials enabled terahertz functional devices. *Nano-Micro Lett.* 2025. **17**. P. 212. https://doi.org/10.1007/s40820-025-01732-1.
4. Guo C., Xu W., Cai M. *et al.* A review: application of terahertz nondestructive testing technology in electrical insulation materials. *IEEE Access*. 2022. **10**. P. 121547–121560. https://doi.org/10.1109/ACCESS.2022.3222860.
5. Greenall N., Valavanis A., Desai H. J. *et al.* The development of a Semtex-H simulant for terahertz spectroscopy. *J. Infrared Millim. Terahertz Waves*. 2017. **38**, No 3. P. 325–338. https://doi.org/10.1007/s10762-016-0336-z.
6. Yang J., Bai X., Wei M. *et al.* Terahertz spectroscopy for food quality assessment: A comprehensive review. *Foods*. 2025. **14**, No 13. P. 2199. https://doi.org/10.3390/foods14132199.
7. Afsah-Hejri L., Akbari E., Toudeshki A. *et al*. Terahertz spectroscopy and imaging: A review on agricultural applications. *Comput. Electron. Agric.* 2020. **177**. P. 105628. https://doi.org/10.1016/j.compag.2020.105628.
8. Baxter J.B., Guglietta G.W. Terahertz spectroscopy. *Anal. Chem*. 2011. **83**, No 12. P. 4342–4368. https://doi.org/10.1021/ac200907z.
9. Ouaras K., Righetti F., Cappelli M. Broadband cw-terahertz spectroscopy for characterizing reactive plasmas. *J. Phys. D: Appl. Phys*. 2019. **52**, No 19. P. 195202. https://doi.org/10.1088/1361-6463/ab085e.
10. Kumar A., Gupta M., Pitchappa P. *et al.* Phototunable chip-scale topological photonics: 160 Gbps waveguide and demultiplexer for THz 6G communication. *Nat. Commun*. 2022. **13**, No 1. P. 5404. https://doi.org/10.1038/s41467-022-32909-6.
11. Jiang W., Zhou Q., He J. *et al.* Terahertz communications and sensing for 6G and beyond: A comprehensive review. *IEEE Commun. Surv. Tutor*. 2024. **26**, No 4. P. 2326–2381. https://doi.org/10.1109/COMST.2024.3385908.
12. Yang Y., Yamagami Y., Yu X. *et al.* Terahertz topological photonics for on-chip communication. *Nat. Photonics*. 2020. **14**, No 7. P. 446–451. https://doi.org/10.1038/s41566-020-0618-9.
13. Nagatsuma T., Ducournau G., Renaud C. Advances in terahertz communications accelerated by photonics. *Nat. Photonics*. 2016. **10**, No 6. P. 371–379. https://doi.org/10.1038/nphoton.2016.65.
14. Fu S., Gao C. *Optical Vortex Beams*. Springer, 2023. https://doi.org/10.1007/978-981-99-1810-2.
15. Ke X. *Generation, Transmission, Detection, and Application of Vortex Beams.* Springer Singapore, 2023. https://doi.org/10.1007/978-981-99-0074-9.
16. Zhou Z., Li P., Ma J. *et al.* Generation and detection of optical vortices with multiple cascaded spiral phase plates. *Photonics*. 2022. **9**, No 5. P. 354. https://doi.org/10.3390/photonics9050354.
17. Cazac V., Achimova E., Abashkin V. *et al.* Polarization holographic recording of vortex diffractive optical elements on azopolymer thin films and 3D analysis via phase-shifting digital holographic

microscopy. *Opt. Express*. 2021. **29**, No 6. P. 9217–9230. https://doi.org/10.1364/OE.415639.
18. Zhang Q., He Z., Xie Z. *et al.* Diffractive optical elements 75 years on: from micro-optics to metasurfaces. *Photonics Insights*. 2023. **2**, No 4. P. R09–R09. https://doi.org/10.3788/PI.2023.R09.
19. Liu J., Duan Y., Li Z. *et al.* Recent progress in nonlinear frequency conversion of optical vortex lasers. *Front. Phys.* 2022. **10**. P. 865029. https://doi.org/10.3389/fphy.2022.865029.
20. Wang D., Le M., Lin S. *et al.* Generation of a mode-tunable optical vortex based on a mirror curvature dynamically controlled Z-shaped resonant cavity. *Opt. Lett*. 2021. **46**, No 13. P. 3079–3082. https://doi.org/10.1364/OL.422316.
21. Wang J., Wan Z., Li, K., Zhang Y. Optical vortex lasers. *Opt Express.* 2025. **33**, No 11. P. 22711–22744. https://doi.org/10.1364/OE.555913.
22. Zhang Z., Hai L., Fu S., Gao C. Advances on solid-state vortex laser. *Photonics*. 2022. **9**, No 4. P. 215. https://doi.org/10.3390/photonics9040215.
23. Yang T.L., Yang J., Li X.P. *et al.* High power nanosecond optical vortex laser oscillation in mode-selection slab resonator. *Appl. Phys. B*. 2024. **130**, No 6. P. 92. https://doi.org/10.1007/s00340-024-08233-w.
24. Mammez M.H., Buchanan Z., Pirali O. *et al.* Optically pumped terahertz molecular laser: Gain factor and validation up to 5.5 THz. *Adv. Photon. Res*. 2022. **3**, No 4. P. 2100263. https://doi.org/10.1002/adpr.202100263.
25. Juppet L., Khabbaz A., Lampin J.F., Pirali O. Terahertz molecular water laser using quantum cascade laser pumping. *J. Appl. Phys*. 2023. **134**, No 24. P. 243101. https://doi.org/10.1063/5.0177191.
26. Sharma S., Singya P.K., Deka K. *et al.* Terahertz communication: State-of-the-art and future directions. *IEEE Open J. Commun. Soc*. 2025. **6**. P. 6281–6322. https://doi.org/10.1109/OJCOMS.2025.3592365.
27. Zhang K., Wang Y., Yuan Y., Burokur S.N. A review of orbital angular momentum vortex beams generation: from traditional methods to metasurfaces. *Appl. Sci*. 2020. **10**, No 3. P. 1015. https://doi.org/10.3390/app10031015.
28. Luneburg R.K. *Mathematical Theory of Optics*. University of California Press, 1964. Sec. 45.7. https://doi.org/10.2307/jj.8501483.
29. Ciattoni A., Crosignani B., Di Porto P. Vectorial analytical description of propagation of a highly nonparaxial beam. *Opt. Commun*. 2002. **202**. P. 17–20. https://doi.org/10.1016/S0030-4018(01)01722-9.
30. Cui X., Wang C., Jia X. Nonparaxial propagation of vector vortex beams diffracted by a circular aperture. *J. Opt. Soc. Am. A*. 2019. **36**, No 1. P. 115–123. https://doi.org/10.1364/JOSAA.36.000115.
31. Agrawal G.P., Pattanayak D.N. Gaussian beam propagation beyond the paraxial approximation. *J. Opt. Soc. Am. A*. 1979. **69**, No 4. P. 575–578. https://doi.org/10.1364/JOSA.69.000575.
32. Liu P., Lü B. The vectorial angular-spectrum representation and Rayleigh–Sommerfeld diffraction formulae. *Opt. Laser Technol*. 2007. **39**, No 4. P. 741–744. https://doi.org/10.1016/j.optlastec.2006.03.006.
33. Jia X., Yang Y., Lu J. Nonparaxial analyses of cylindrical vector beams with arbitrary polarization order in the far field. *J. Mod Opt*. 2016. **63**, No 16. P. 1544–1551. https://doi.org/10.1080/09500340.2016.1160156.
34. Marcatili E.A.J., Schmeltzer R.A. Hollow metallic and dielectric waveguides for long distance optical transmission and lasers. *Bell Syst. Techn. J*. 1964. **43**, No 4. P. 1783–1809. https://doi.org/10.1002/j.1538-7305.1964.tb04108.x.
35. Nye J.F., Berry M.V. Dislocations in wave trains. *Proc. R. Soc. Lond. A. Math. Phys. Sci.* 1974. **336**, No 1605. P. 165–190. https://doi.org/10.1098/rspa.1974.0012.
36. Wang H., Song Q., Cai Y. *et al.* Recent advances in generation of terahertz vortex beams and their applications. *Chin. Phys. B*. 2020. **29**, No 9. P. 097404. https://doi.org/10.1088/1674-1056/aba2df.
37. Gu B., Cui Y. Nonparaxial and paraxial focusing of azimuthal-variant vector beams. *Opt. Express*. 2012. **20**, No 16. P. 17684–17694. https://doi.org/10.1364/OE.20.017684.
38. Gurin O.V., Degtyarev A.V., Dubinin N.N. *et al.* Formation of beams with nonuniform polarisation of radiation in a cw waveguide terahertz laser. *Quantum Electron*. 2021. **51**, No 4. P. 338. https://doi.org/10.1070/QEL17511.

Authors and CV

Andrey V. Degtyarev, PhD in Physics and Mathematics, Associate Professor, Department of Quantum Radiophysics, School of Radiophysics, Biomedical Electronics and Computer Systems, V.N. Karazin Kharkiv National University.
Authored over 80 scientific works, several methodical training manuals, three monographs, and a patent for an invention. The field of his scientific interests is laser physics, laser optics, and propagation of laser radiation beams in electromagnetic energy transmission lines.
E-mail: a.v.degtyarev@karazin.ua,
https://orcid.org/0000-0003-0844-4282

Mykola M. Dubinin, PhD in Applied Physics and Nanomaterials, Department of Quantum Radiophysics, School of Radiophysics, Biomedical Electronics and Computer Systems, V.N. Karazin Kharkiv National University. He is the author of more than 30 scientific works, 2 monographs and a patent for an invention. The field of his scientific interests is laser physics, laser optics, and propagation, focusing and control of laser radiation beams. https://orcid.org/0000-0002-7723-9592

Oleg V. Gurin (1961–2025), Researcher, Department of Quantum Radiophysics, School of Radiophysics, Biomedical Electronics and Computer Systems, V.N. Karazin Kharkiv National University. His research activity focused on experimental studies of submillimeter laser systems, including the formation of beams with uniform intensity distribution and transverse mode selection in laser cavities. He was the author of more than 40 scientific publications and six innovations.
https://orcid.org/0000-0003-1382-5338

Vyacheslav O. Maslov, Doctor of Physical and Mathematical Sciences, Professor, Department of Quantum Radiophysics, School of Radiophysics, Biomedical Electronics and Computer Systems, V.N. Karazin Kharkiv National University. He is the author of more than 200 scientific works, 6 monographs, several methodical training manuals, and 18 copyright certificates for inventions and patents. The field of his scientific interests is laser physics, laser optics, and propagation of laser radiation beams in electromagnetic energy transmission lines. https://orcid.org/0000-0001-7743-7006, e-mail: v.a.maslov@karazin.ua

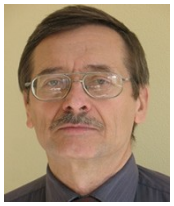

Konstantin I. Muntean, PhD Student, Department of Quantum Radiophysics, School of Radiophysics, Biomedical Electronics and Computer Systems, V.N. Karazin Kharkiv National University. He is the author and co-author of more than 130 scientific publications, including 15 copyright certificates and patents for inventions. The field of his scientific interests is measurements and stabilization of laser radiation parameters.
E-mail: k.i.muntean@karazin.ua,
https://orcid.org/0000-0001-6479-3511

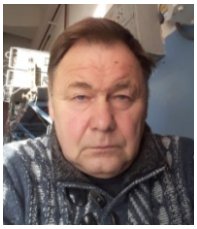

Valery N. Ryabykh, Researcher, Department of Quantum Radiophysics, School of Radiophysics, Biomedical Electronics and Computer Systems, V.N. Karazin Kharkiv National University. He is the author and co-author of about 30 publications and holds 5 inventor's certificates. His research interests include waveguide optics, beam propagation and mode control, optical sensing, and envi-ronmental diagnostics.
E-mail: v.ryabykh@karazin.ua,
https://orcid.org/0000-0002-3526-292X

Authors' contributions

Degtyarev A.V.: formal analysis, project administration, writing – review & editing.
Dubinin M.M.: methodology, investigation, writing – review & editing.
Gurin O.V.: investigation, formal analysis.
Maslov V.A.: formal analysis, conceptualization, investigation, writing – original draft, writing – review & editing.
Muntean K.I.: validation, formal analysis
Ryabykh V.N.: investigation, formal analysis.

Динаміка поширення радіально поляризованих терагерцових вихрових пучків

А.В Дегтярьов, М.М. Дубінін, О.В. Гурін, В.О. Маслов, К.І. Мунтян, В.М. Рябих

Анотація. Отримано аналітичні вирази для опису непараксіальної дифракції вихрових лазерних пучків під час їхнього поширення у вільному просторі. Розглянуто пучки, збуджені радіально поляризованими TM_{0m} (m = 1, 2, 3) модами діелектричного хвилевідного резонатора терагерцового лазера, які взаємодіють зі спіральною фазовою пластинкою з довільним топологічним зарядом (n). Моделювання виконано за допомогою інтегральної теорії Релея–Зоммерфельда. Показано, що фазова пластинка з топологічними зарядами n = 1, 2 формує в зоні Френеля поле, в якому з'являється азимутальна компонента. Радіальна та поздовжня компоненти зберігаються, причому внесок поздовжньої компоненти у сумарну потужність залишається незначним. Для заряду n = 1 максимум інтенсивності поля розташований на осі, тоді як для n = 0 і n = 2 розподіл поля набуває кільцевої структури. Максимальні значення інтенсивності спостерігаються при n = 1, тоді як для n = 2 вони зменшуються. Візуалізовано фазові розподіли поперечних компонент поля вихрових лазерних пучків. Для топологічного заряду n = 1 спостерігається їх однопелюсткова гвинтоподібна структура, а для n = 2 – двопелюсткова з більш вираженими спіральними закрутками азимутальної компоненти для всіх досліджуваних мод.

Ключові слова: вихровий пучок, терагерцовий лазер, діелектричний резонатор, моди, фазова пластинка, поширення.